Electronic Supplementary Material (ESI) for Journal of Materials Chemistry A.

Enhanced N_2 Affinity of 1T-MoS_2 with Unique Pseudo Six-membered Ring Consisting of N—Li—S—Mo—S—Mo for High Ambient Ammonia Electrosynthesis Performance

Shivaraj B. Patil,[1#] Hung-Lung Chou,[2#] Yu-Mei Chen,[1] Shang-Hsien Hsieh,[3] Chia-Hao Chen,[3] Chia-Che Chang,[1] Shin-Ren Li,[1] Yi-Cheng Lee,[1] Ying-Sheng Lin,[1] Hsin Li,[1] Yuan Jay Chang,[1] Ying-Huang Lai,[1] Di-Yan Wang[1]*

[1] Department of Chemistry, Tunghai University, Taichung 40704, Taiwan

[2] Graduate Institute of Applied Science and Technology, National Taiwan University of Science and Technology, Taipei 10607, Taiwan

[3] National Synchrotron Radiation Research Center, Hsinchu 30076, Taiwan

[#]Shivaraj B. Patil and Hung-Lung Chou are contributed equally to this work

Corresponding author: diyanwang@thu.edu.tw

Table S1. Adsorption energies and optimized geometries calculation of H in MoS_2 with Li and without Li systems

	E_{ad} (eV)	E_{ad} (eV)	Distance (S-H) (Å)
S site of MoS_2 (with Li-S)	0.492	0.47[3]	1.381 (± 0.02 Å)
S site of MoS_2 (without Li-S)	0.034	0.03[3]	1.383 (± 0.02 Å)

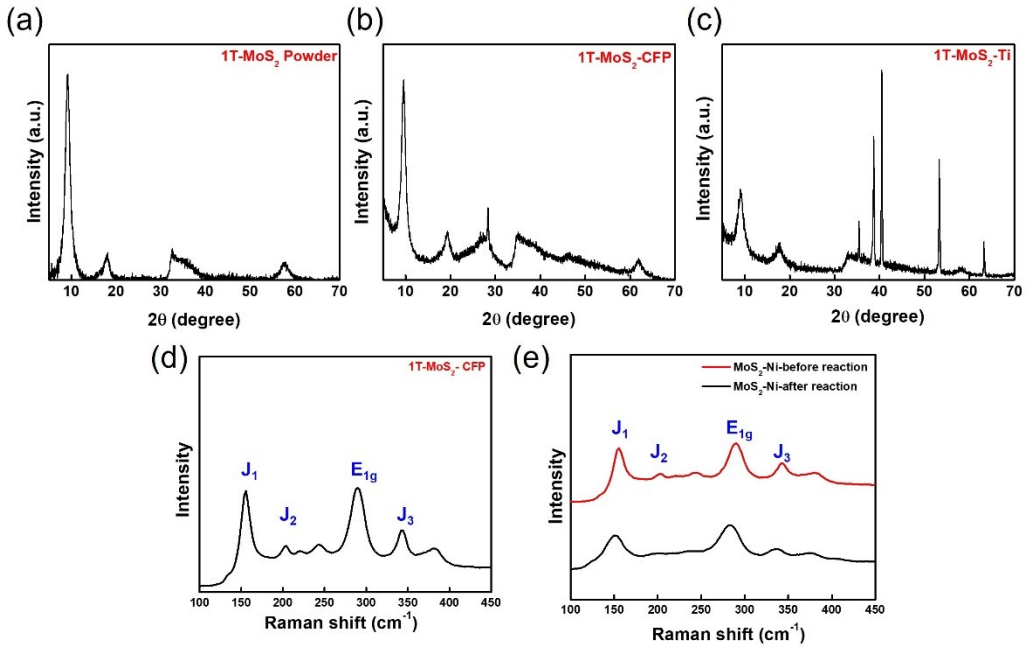

Figure S1. (a-c) XRD patterns of 1T-MoS_2-powder, 1T-MoS_2-CFP and 1T-MoS_2-Ti, respectively; (d-e) Raman spectra of 1T-MoS_2-CFP and 1T-MoS_2-Ni, respectively. Similar kind of XRD pattern having sharp peaks was also obtained for 1T-MoS_2 powder when synthesized without any substrates. Therefore, it is evident that Ni foil exhibits duel nature, that is, acting as suitable substrate and amorphization agent. Meanwhile, Raman spectra confirms the formation of distorted amorphous 1T-MoS_2 and maintains same phase after the reactions also.

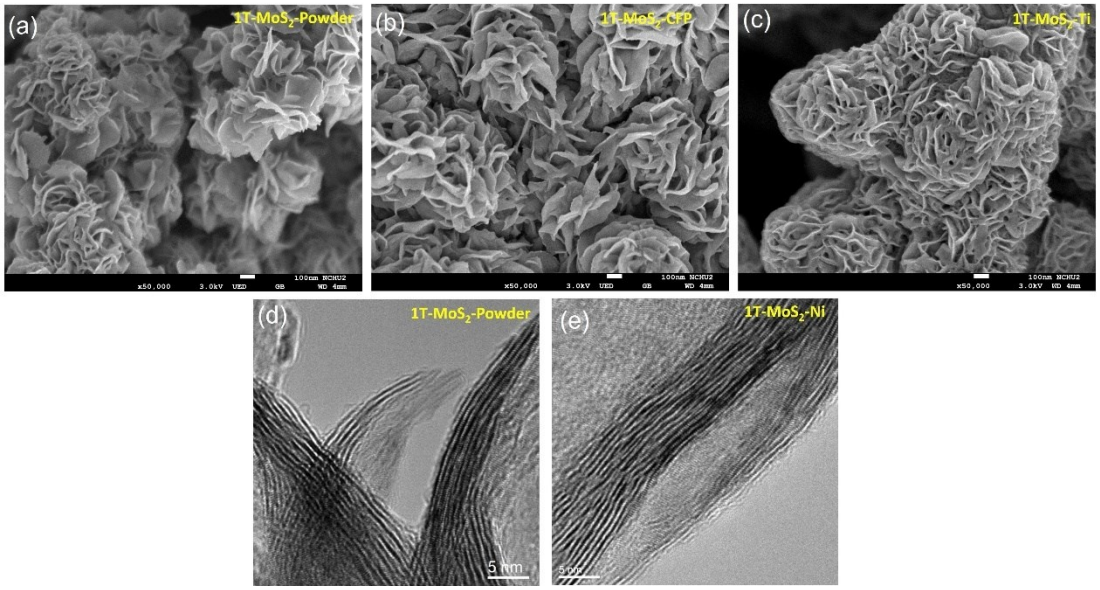

Figure S2. (a-c) SEM images of 1T-MoS_2-powder, 1T-MoS_2-CFP and 1T-MoS_2-Ti, respectively; (d-e) HR-TEM image of 1T-MoS_2-powder and 1T-MoS_2-Ni, respectively. These 1T-MoS_2 catalysts exhibited high crystalline beautiful nanoflower morphology. FE-SEM images further substantiate the significant role of Ni in amorphization of 1T-MoS_2. The d-spacing calculated from the HR-TEM corresponds to 1T phase of MoS_2. HR-TEM image reveals the formation of defective amorphous 1T-MoS_2.

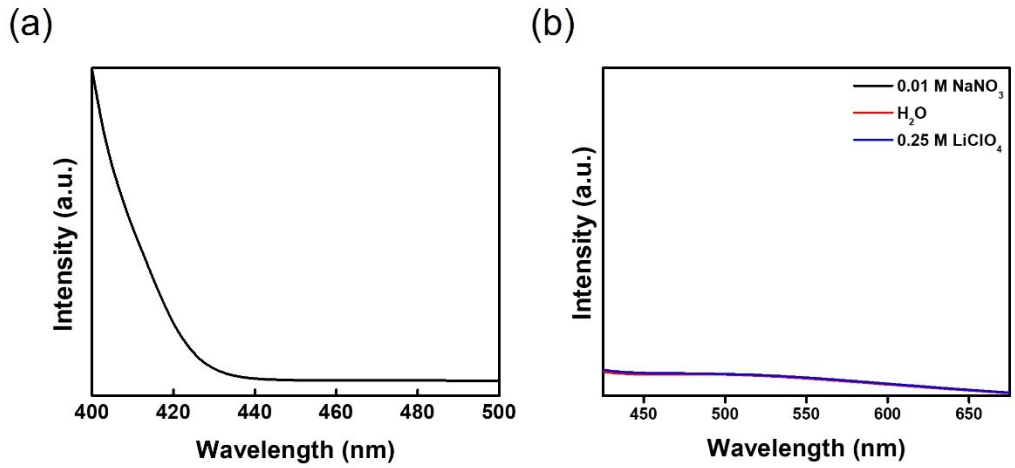

Figure S3. (a) UV-vis absorption spectra of the electrolyte stained with Watt and Chrisp indicator after NRR electrolysis using 1T-MoS_2-Ni at -0.3 V. The result rules out the formation of hydrazine and signifies the formation of NH_3 only. (b) UV-vis absorption spectra of the electrolytes stained with Griess reagent (equal volumes of electrolyte and reagent were mixed and read the absorbance at 540 nm after 15 min).

To validate the results are real, many controlled experiments were carried out. **Figure S10 (a)** shows UV-vis absorption spectra of pure electrolyte with purging N_2 and Ar gas stained with indophenol indicator. **Figure S10 (b)** shows the gas chromatography of N_2 gas. It was found that there is no contamination either from the electrolyte or gas. **Figure 11S (a & b)** show time dependent current curves and corresponding UV-Vis spectra of 1T-MoS_2-Ni using carbon as a counter electrode. The efficiency remains almost same signifying the non-interference of Pt ions. **Figure 11S (c & d)** show time dependent current curves and corresponding UV-Vis spectra of 1T-MoS_2-Ni using Li_2SO_4 electrolyte. Unbowed efficiency indicates the insignificant effect of anions on the performance of 1T-MoS_2-Ni. No ammonia was detected when Ni with and without catalyst exposed to chronoamperometric tests in Ar atmosphere [**Figure 11S (e & f)**] confirming that no contamination originated from electrode.

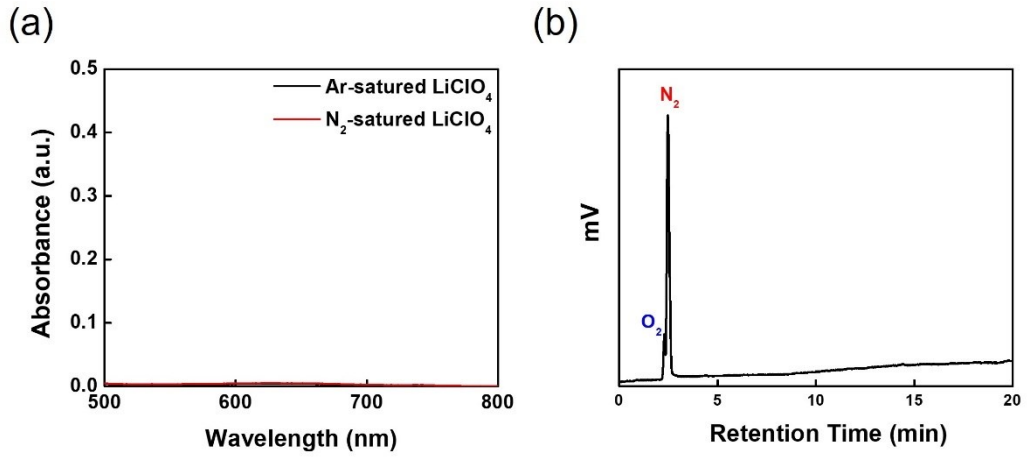

Figure S4. (a) UV-vis absorption spectra of pure electrolyte with purging N_2 and Ar gas stained with indophenol indicator. It was found that there is no contamination either from the electrolyte. **(b)** Gas chromatography of N_2 gas.

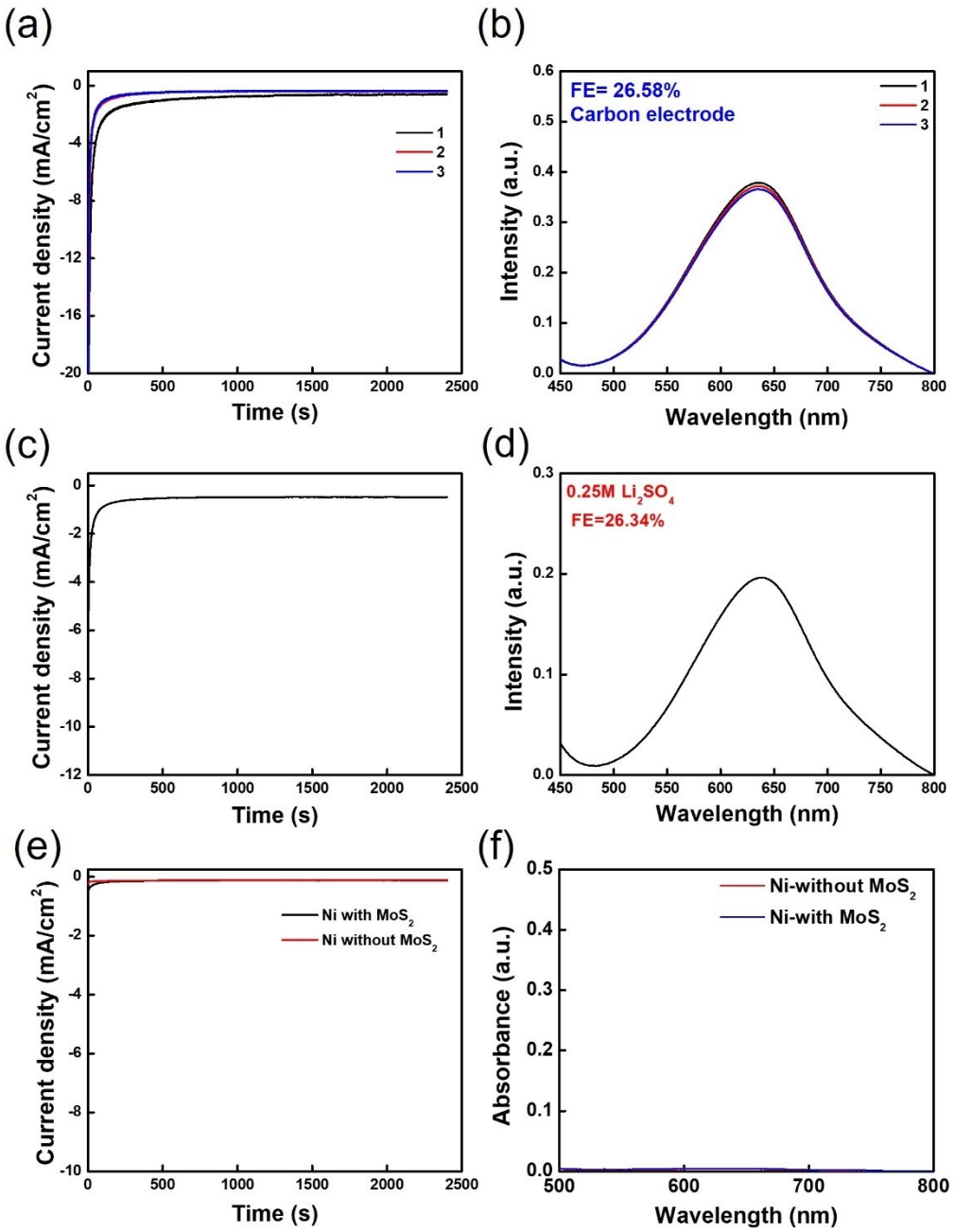

Figure S5. (a & b) Time dependent current curves and corresponding UV-vis absorption spectra of 1T-MoS_2-Ni for consecutive cycles using carbon rod as a counter electrode to study the effect of Pt counter electrode in H-type cell; **(c & d)** Time dependent current curves and corresponding UV-vis absorption spectra of 1T-MoS_2-Ni operated in 0.25 M Li_2SO_4 electrolyte; **(e & f)** Time dependent current curves (Ar atmosphere) and corresponding UV-vis absorption spectra of Ni with and without MoS_2 at -0.3V vs RHE.

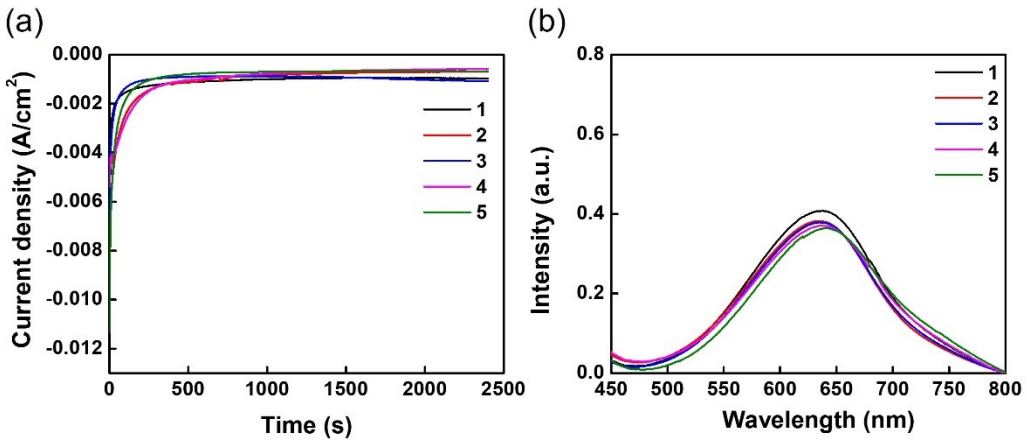

Figure S6. (a) Time dependent current curves of 1T-MoS_2-Ni for consecutive cycles. (b) UV-vis absorption spectra of the electrolyte stained with indophenol indicator after NRR electrolysis using 1T-MoS_2-Ni for consecutive cycles.

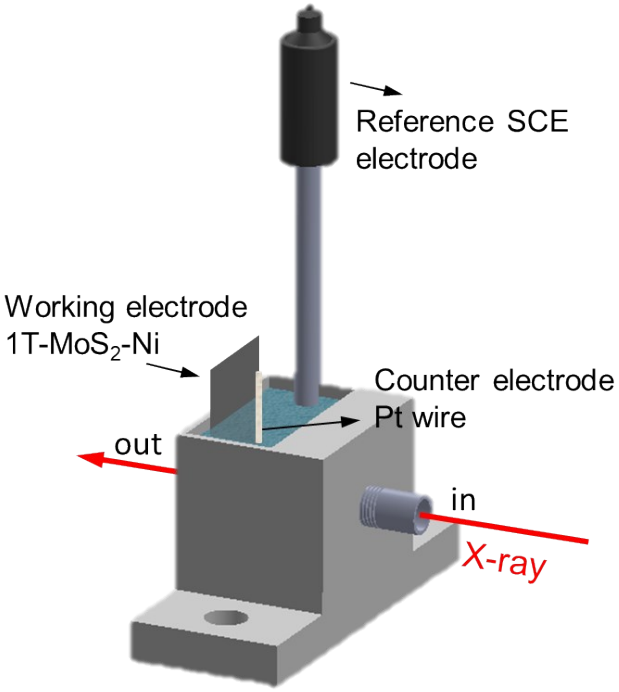

Figure S7. The setup of electrochemical reaction of in-situ XRD- measurement.

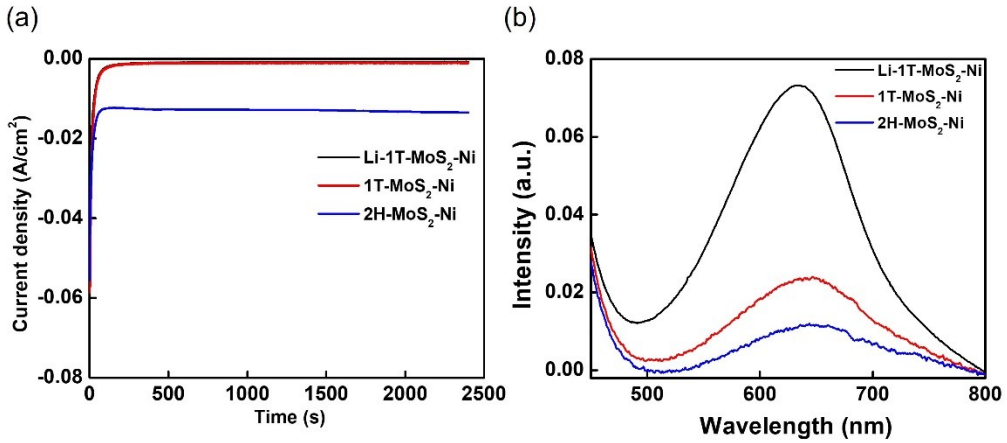

Figure S8. (a) Time dependent current curves of different catalysts operated in 0.25 M Na_2SO_4 electrolyte. (b) UV-vis absorption spectra of the corresponding electrolytes stained with indophenol indicator.

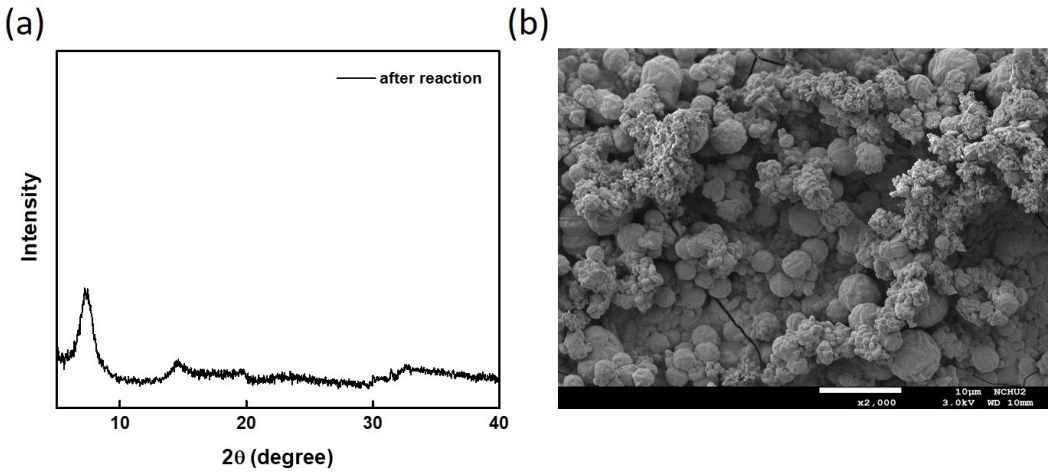

Figure S9: (a-b) XRD pattern and SEM image of 1T-MoS_2 after NRR, respectively.

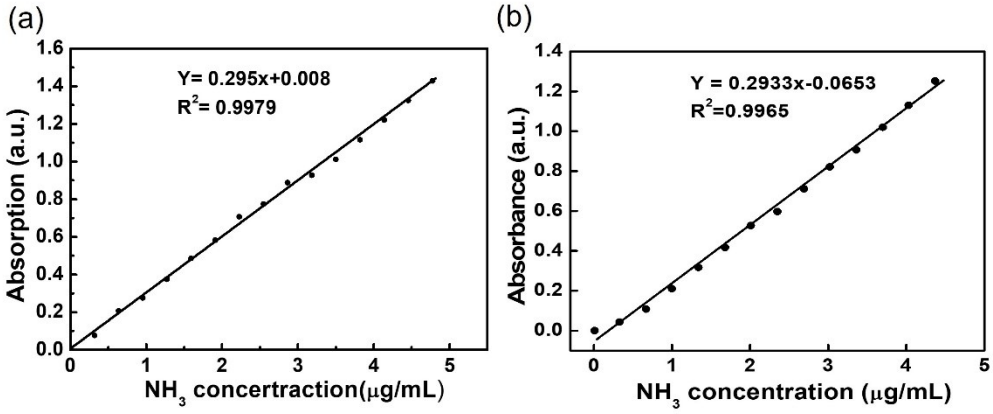

Figure S10. The calibration curves used to quantify the NH_3 generated during electrolysis for (a) $LiClO_4$ and (b)Na_2SO_4 electrolytes, respectively.

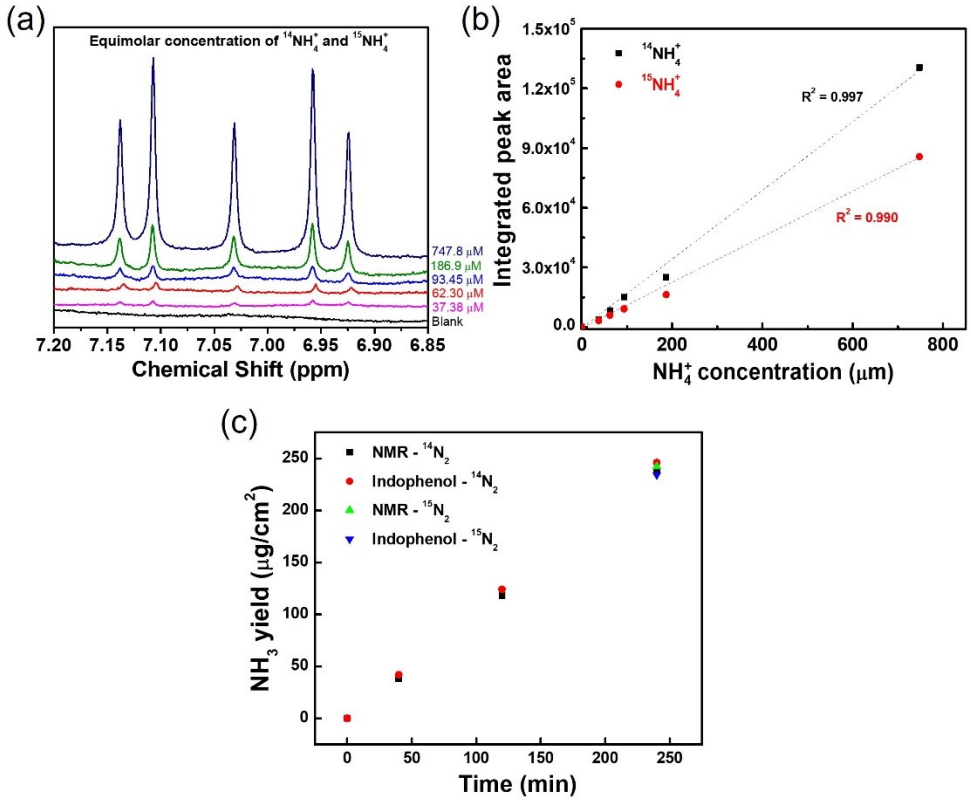

Figure S11. (a) NMR spectra of equimolar concentrations of $^{14}NH_4^+$ and $^{15}NH_4^+$. The slight deviation of chemical shift can be attributed to difference s in pH, volume and/or temperature. (b) NMR based calibration curve used to quantify the NH_3 generated during electrolysis. (c) NH_3 yield obtained by both indophenol and NMR over different periods.

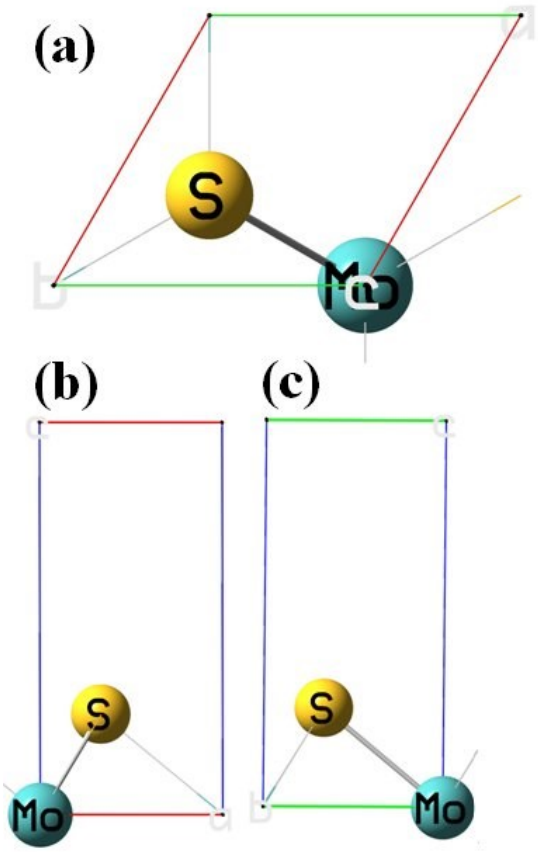

Figure S12. The models of unit cell of 1T-MoS_2 in the (a) top-view, and (b) side-view (along x-axis), and (c) side-view of MoS_2 (along y-axis).

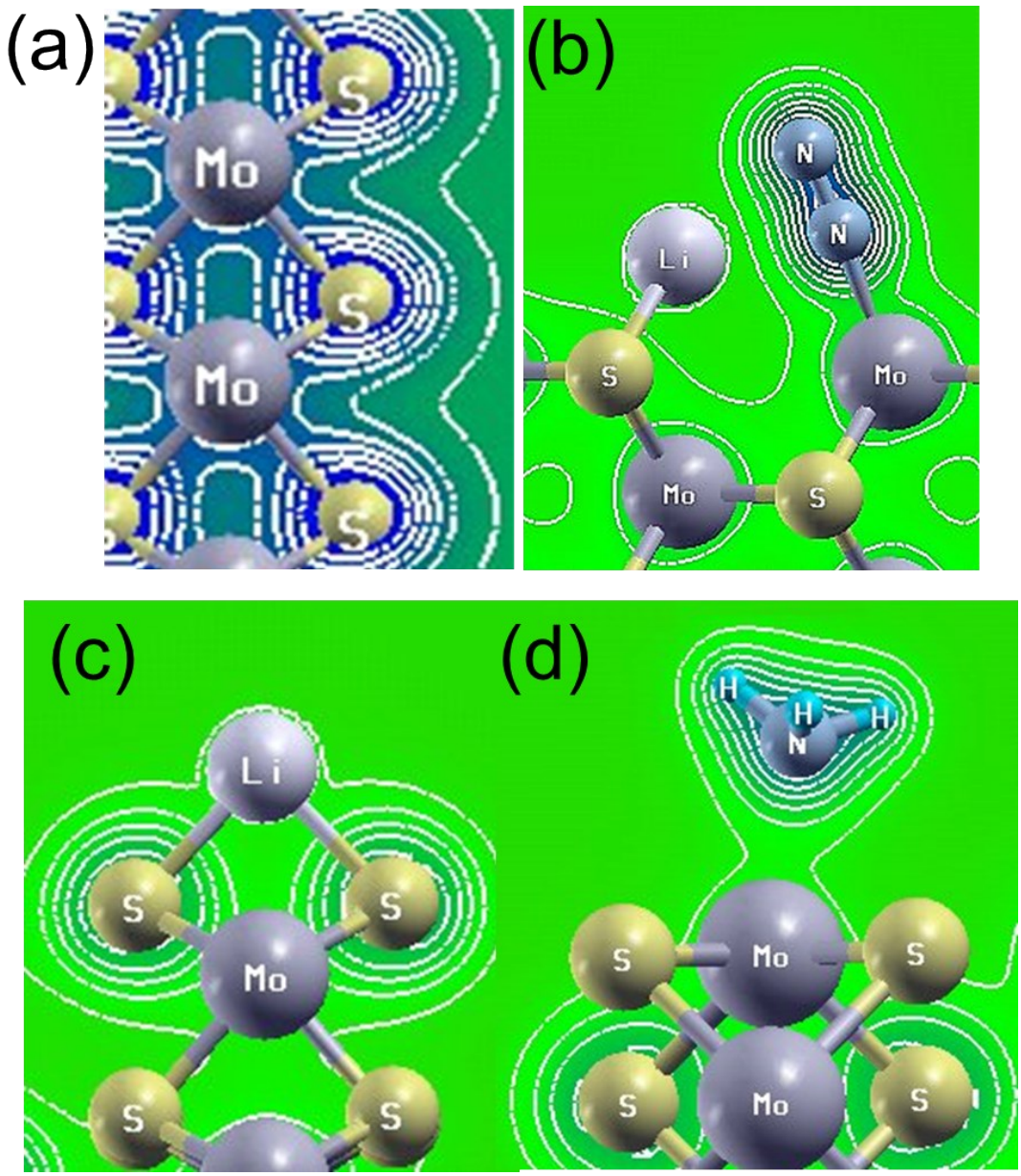

Figure S13. (a) The electron contour map obtained from the top-view. (b) The key structures of intermediates N=N adsorbed with Li-S on MoS_2 of the PED. (c) The key structures of intermediates Li adsorbed on bridge-S on MoS_2. (d) The electron contour map of Mo-NH_3 from the side-view.

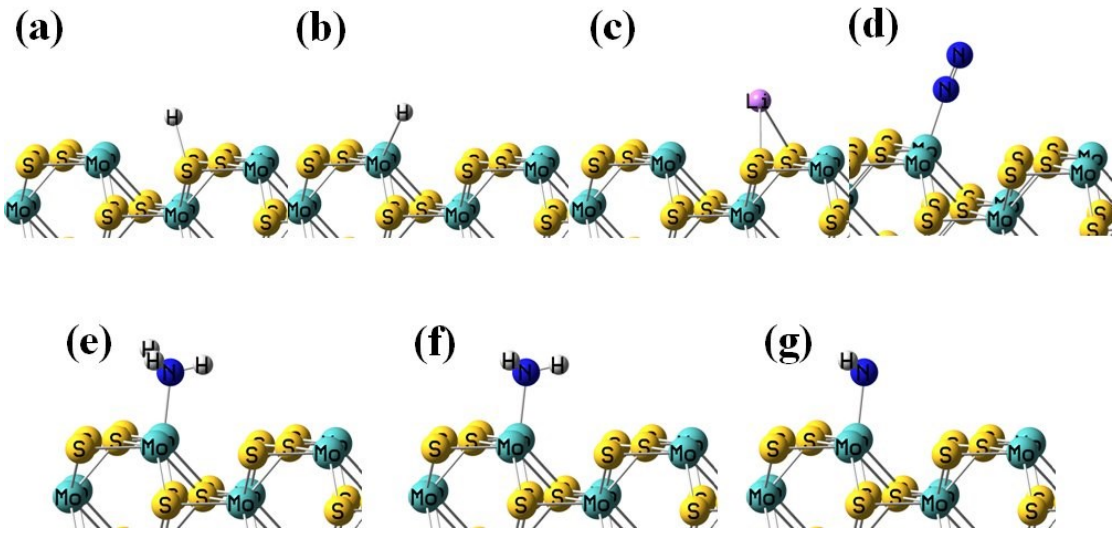

Figure S14. The Side-view of the 1T-MoS_2 edges. (a) H* adsorption on the S-edge site and (b) H* adsorption on the Mo-edge site and (c) Li* adsorption on the bridge S site and (d) N_2* adsorption on the Mo site and (e) NH_3* adsorption on the Mo site and (f) NH_2* adsorption on the Mo site and (g) NH_1* adsorption on the Mo site.

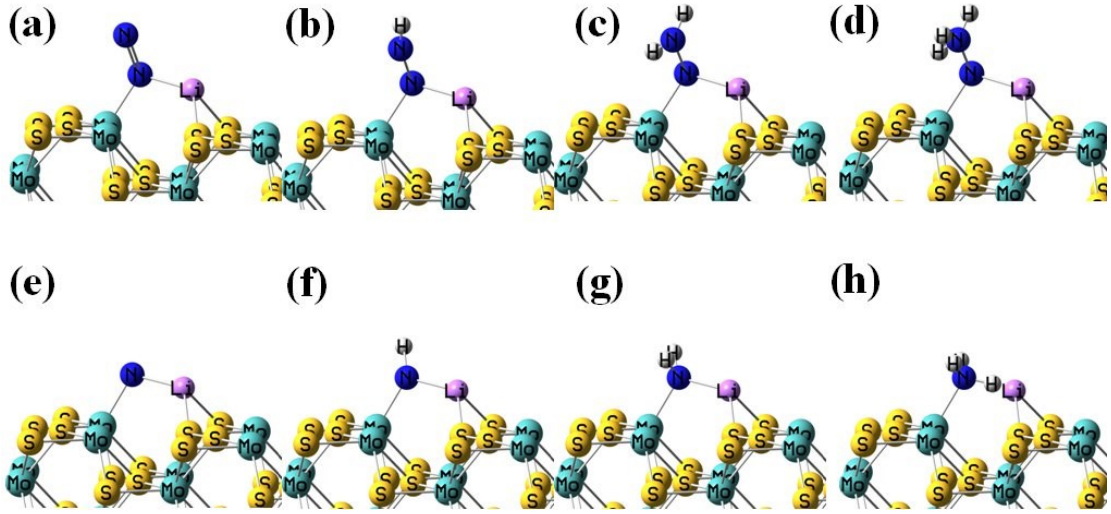

Figure S15. The geometries of the initial states (I. S.) for (a) nitrogen adsorption and nitrogen reduction reaction (NRR), the intermediate states (I. M. S.) (b)-(g), and the final states (F. S.), and (h) final states (F.S.) for NH_3 adsorption on the Li-1T-MoS_2.

Table S2: The literatures of other metal sulfide electrocatalysts for NRR in comparison with our work.

Compounds name	Electrolytes	RHE (V)	NH_3 yield rate ($\mu g/h/mg_{cat}$)	Faradaic efficiency (%)	Ref.
1T-MoS_2-Ni	**0.25 M $LiClO_4$**	**-0.3**	**1.05 μg/min/cm²**	**27.66**	**Present**
Ru-MoS_2	10 mM HCl	-0.15	0.11 nmol/s/cm²	17.60	[1]
Co-MoS_2	0.01 H_2SO_4	-0.3	0.63 nmol/h/g	10.00	[2]
MoS_2	0.1 M $LiSO_4$	-0.2	43.4	9.81	[3]
N-MoS_2	0.1 M Na_2SO_4	-0.3	69.82	9.14	[4]
DR-MoS_2	0.1 M Na_2SO_4	-0.4	29.28	8.34	[5]
2H-MoS_2	0.1 M Na_2SO_4	-0.5	0.08 nmol/s/cm²	1.17	[6]
MoS_2-rGO	0.1 M $LiClO_4$	-0.45	24.82	4.56	[7]
FeS_x/Fe	0.1 M KOH	-0.3	0.41 nmol/s/cm²	17.60	[8]
FeS_2	$LiSO_{4\ (pH=2)}$	-0.2	11.5	14.60	[9]
FeS_2/CFP	0.25 M $LiClO_4$	-0.6	0.096 μg/min	14.14	[10]
Fe_3S_4	0.1 M HCl	-0.4	75.4	6.45	[11]
Sn/SnS_2	0.1 M PBS	-0.7	23.8	6.50	[12]
SnS_2/ZnS_2@Ni	0.1 M Na_2SO_4	-0.5	0.91 nmol/s/cm²	10.80	[13]

References

1. Suryanto BH*, et al.* MoS_2 polymorphic engineering enhances selectivity in the electrochemical reduction of nitrogen to ammonia. *ACS Energy Letters* **4**, 430-435 (2018).

2. Zhang J*, et al.* Cobalt-Modulated Molybdenum–Dinitrogen Interaction in MoS_2 for Catalyzing Ammonia Synthesis. *Journal of the American Chemical Society* **141**, 19269-19275 (2019).

3. Liu Y*, et al.* Dramatically Enhanced Ambient Ammonia Electrosynthesis Performance by In-Operando Created Li–S Interactions on MoS_2 Electrocatalyst. *Advanced Energy Materials* **9**, 1803935 (2019).

4. Zeng L, Chen S, van der Zalm J, Li X, Chen A. Sulfur vacancy-rich N-doped MoS_2 nanoflowers for highly boosting electrocatalytic N_2 fixation to NH_3 under ambient conditions. *Chemical Communications* **55**, 7386-7389 (2019).

5. Li X*, et al.* Boosted electrocatalytic N_2 reduction to NH_3 by defect-rich MoS_2 nanoflower. *Advanced Energy Materials* **8**, 1801357 (2018).

6. Zhang L*, et al.* Electrochemical ammonia synthesis via nitrogen reduction reaction on a MoS_2 catalyst: theoretical and experimental studies. *Advanced Materials* **30**, 1800191 (2018).

7. Li X*, et al.* A MoS_2 nanosheet–reduced graphene oxide hybrid: an efficient electrocatalyst for electrocatalytic N_2 reduction to NH_3 under ambient conditions. *Journal of materials chemistry A* **7**, 2524-2528 (2019).

8. Xiong W, Guo Z, Zhao S, Wang Q, Xu Q, Wang X. Facile, cost-effective plasma synthesis of self-supportive FeS_x on Fe foam for efficient electrochemical reduction of N_2 under ambient conditions. *Journal of Materials Chemistry A* **7**, 19977-19983 (2019).

9. Feng D, Zhang X, Sun Y, Ma T. Surface-defective FeS_2 for electrochemical NH3 production under ambient conditions. *Nano Materials Science*, (2019).

10. Chang CC*, et al.* Photoactive Earth-Abundant Iron Pyrite Catalysts for Electrocatalytic

Nitrogen Reduction Reaction. *Small* **15**, 1904723 (2019).

11. Zhao X, Lan X, Yu D, Fu H, Liu Z, Mu T. Deep eutectic-solvothermal synthesis of nanostructured Fe_3S_4 for electrochemical N_2 fixation under ambient conditions. *Chemical communications* **54**, 13010-13013 (2018).

12. Li P*, et al.* Amorphous Sn/Crystalline SnS_2 Nanosheets via In Situ Electrochemical Reduction Methodology for Highly Efficient Ambient N_2 Fixation. *Small* **15**, 1902535 (2019).

13. Chen X, Liu Y-T, Ma C, Yu J, Ding B. Self-organized growth of flower-like SnS_2 and forest-like ZnS nanoarrays on nickel foam for synergistic superiority in electrochemical ammonia synthesis. *Journal of Materials Chemistry A* **7**, 22235-22241 (2019).